Mechanism of 1,4,5,8-naphthalene tetracarboxylic acid dianhydride hydrolysis and formation in aqueous solution

T. C. Barros,[a] I. M. Cuccovia,*[c] J. P. S. Farah,[b] J. C. Masini,[b] H. Chaimovich[c] and M. J. Politi[c]

Received 30th August 2005, Accepted 1st November 2005
First published as an Advance Article on the web 18th November 2005
DOI: 10.1039/b512187f

The study of highly conjugated, carbonyl-containing molecules such as 1,4,5,8-naphthalene tetracarboxylic dianhydride, **III**, is of interest since reactivity differences and transmission of electronic effects through the conjugated framework can be evidenced. The kinetics of hydrolysis of **III** in aqueous solution were determined from 5 M acid to pH 10. In basic solution hydrolysis of **III** yields, sequentially, 1,4,5,8-naphthalene diacid monoanhydride, **II**, and 1,4,5,8-naphthalene tetracarboxylic acid, **I**. The second order rate constant for alkaline hydrolysis is 200 fold higher for the first ring opening. The water-catalyzed hydrolysis of **III** yields a pH-dependent mixture of ionic forms of **I** and **II**. The rate constant for water-catalyzed hydrolysis of **III** is 25 fold higher than that for **II**. In concentrated acid the rates for reaching equilibrium (**I**, **II** and **III**) increase and **III** is the major product. The pK_as of **I** (3.24, 5.13 and 6.25) and **II** (3.05, 5.90) were determined by potentiometric, fluorescence and UV spectroscopy titrations and by quantitative fit of the kinetic and equilibrium data. The apparent, pH-dependent, equilibrium constants, K_{EqII}, for anhydride formation between **I** and **II** were obtained from the UV spectra. The quantitative fit of kinetic and equilibrium data are consistent with the assumption that anhydride formation only proceeds with the fully protonated species for both **I** and **II** and permitted the estimation of the equilibrium constants for anhydride formation, K_{EqII}. The value of K_{EqII} (**I** $\rightleftharpoons$ **II**) between pH 1 and 6 was *ca.* 5. Geometry optimization calculations in the gas phase of the reactions of **III** in alkaline, neutral and acid conditions, at the DFT level of theory, gave electronic distributions that were qualitatively consistent with the experimental results.

1 Introduction

The experimental and theoretical analysis of anhydride formation in intramolecular reactions is a paradigmatic model chemical system, extensively used to analyze ground and transition state contributions to the rates of intramolecular and enzymatic reactions.[1]

Hydrolysis of carboxylic anhydrides in aqueous solution can be spontaneous, acid or base-catalyzed.[1–6] Dicarboxylic acids can be in equilibrium with the correspondent anhydrides in aqueous solutions and, in general, the equilibrium is displaced towards the diacid.[7,8] The equilibrium constant may vary from 10^{-7} to 25 depending on structure and the unionized diacid is the kinetically significant species for anhydride formation.[7–9]

The equilibrium between 1,8-naphthalic anhydride, 1,8-An, and its hydrolysis product 1,8-naphthalene dicarboxylic acid, 1,8-Acid, in aqueous solution has been analyzed previously.[10] The pH dependence of hydrolysis kinetics of 1,8-An is complex and indicates an equilibrium reaction between 1,8-An and 1,8-Acid at pHs lower than 5.0. Kinetics and equilibrium results were rationalized by assuming that protonated forms of the 1,8-Acid are in equilibrium with 1,8-An. The values of the equilibrium constants for 1,8-An formation range from 4, between pH 0 and 6, to 100 in concentrated acid. *Ab initio* calculations for the pathway connecting the undissociated 1,8-Acid to the 1,8-An are consistent with a mechanism involving a rate determining intramolecular proton transfer concerted with oxygen alignment towards the carbonyl center forming a transition state with a neutral and planar intermediate with an sp^3 carbon. The second step is dehydration, through another transition state, yielding a complex between water and 1,8-An.[10]

Tetra-substituted naphthalene acid, namely 1,4,5,8-naphthalene tetracarboxylic acid, **I**, Scheme 1, and its mono **II** and dianhydrides, **III**, are intermediates in the synthesis of polymers and dyes.[11]

Fully protonated **I** yields 1,4,5,8-naphthalene tetracarboxylic dianhydride, **III**, upon drying.[11] Hydrolysis of **III** in aqueous base was reported to yield **I** without the formation of 1,4,5,8-naphthalene diacid monoanhydride, **II**, as an intermediate, Scheme 1.[11] Compound **II** was obtained by acidification of **I** with mineral acid at temperatures above 60 °C. Kofman and coworkers prepared **I**, and its derivatives, **II** and **III**, in acid at 90 °C and 140–150 °C, respectively.[11] Acid dissociation constants and alkaline hydrolysis in aqueous DMSO were also analyzed.[11] Compounds **I**, **II** and **III** showed 4, 3 and 2 dissociable groups, respectively, and the authors rationalized the data by assuming an intermediate, formed after OH^- attack at carbonyl groups of **III**, leads to the appearance of a dissociable group and the opening of the two anhydrides to yield **I**. The formation of **II** in aqueous solution upon heating was suggested from NMR spectra and it was proposed that, in moist DMSO, an equilibrium between **I** and

[a]*Universidade Paulista, Instituto de Ciências da Saúde, Bauru, SP, Brazil*
[b]*Departamento de Química Fundamental and Instituto de Química da, Universidade de São Paulo, SP, Brazil*
[c]*Departamento de Bioquímica do, Instituto de Química da, Universidade de São Paulo, SP, Brazil. E-mail: imcuccov@quim.iq.usp.br*

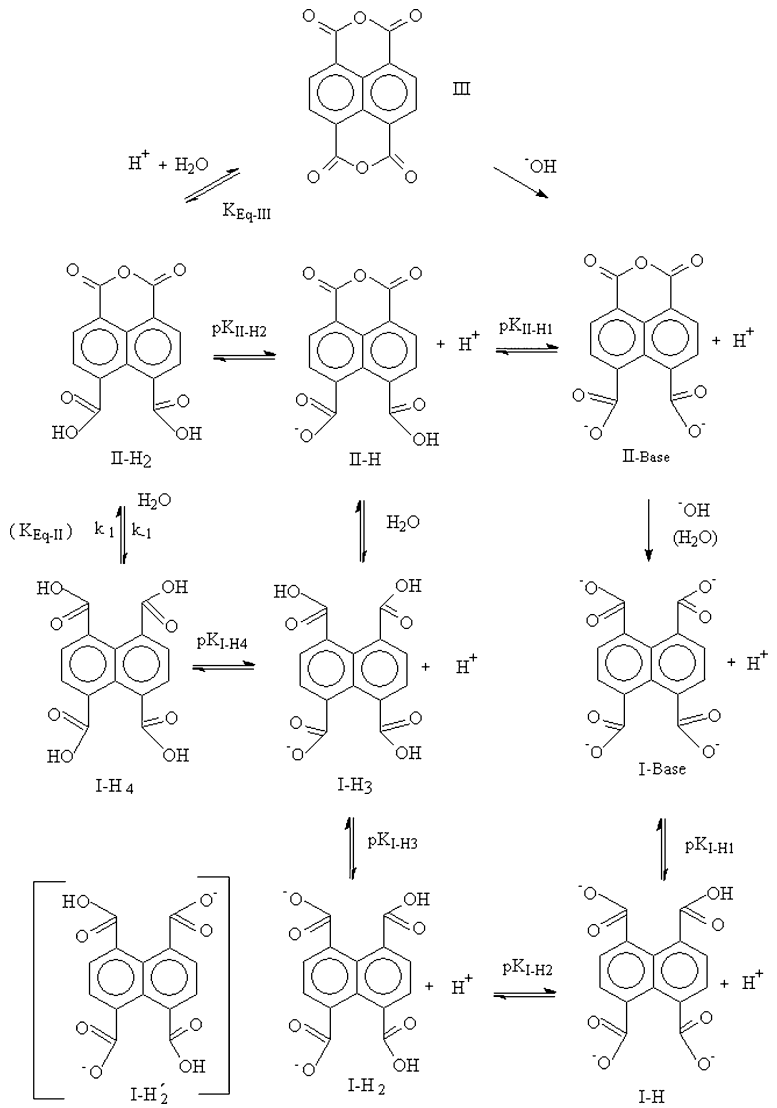

Scheme 1 Reactions involved in the hydrolysis of **III** to **II** and **I**.

III is possible.[12] Crystal structures of compounds **I**, **II** and **III** are known.[12–16]

1,4,5,8-Naphthalene tetracarboxylic acid, **I**, Scheme 1, is an interesting model where short-range electronic and steric interactions, as well as protonation states, can modulate chemical reactivity. Intramolecular reactions of **I** exhibit short range interactions that are typical of those encountered in an enzyme active site.

The detailed pathways of anhydride formation and hydrolysis in the 1,4,5,8-naphthalene tetracarboxylic system have not been analyzed. It seemed unlikely that the hydrolysis of **III** yielded **I** without the intervening formation of **II**, as described previously.[11] Here we present kinetic and equilibrium data that contribute to the understanding of the mechanism of formation and hydrolysis of **III** in aqueous solutions. Cyclization of **I** to **II** and further cyclization to **III**, in acid, were also studied. The p*K*s of **I** and **II** were determined using UV-Vis and fluorescence spectroscopy, potentiometric titration and kinetic data. Cyclization of both **I** and **II** depends on the protonation of the carboxylic groups. Geometry optimization of **III**, selected intermediates and monoanhydrides was performed to define differences in reactivity between the mono and dianhydrides in the acid, water and base-catalyzed reactions.

2 Experimental

2.1 Materials

1,4,5,8-Naphthalene tetracarboxylic dianhydride, **III**, (Aldrich) was used without further purification. The tetra sodium salt of 1,4,5,8-naphthalene tetracarboxylic acid,[17] **I-Base**, (Scheme 1) was prepared by alkaline hydrolysis of **III**, adding **III** to yield a final concentration of 0.001 M in aqueous solutions of NaOH and maintaining the sample at 30 °C for 30 min (see results). At the end of the reaction, absorbance measurement at 368 nm guaranteed complete hydrolysis of **III** to **I-Base** (see results).

1,4,5,8-Naphthalene diacid monoanhydride, **II**: 12.5 mL of an aqueous solution of **I-Base** (1×10^{-3} M) in NaOH (0.005 M) was added to a 25 mL volumetric flask containing water and HCl sufficient to give pH 1.0 and 5×10^{-4} M of protonated **I-Base**,

I-H$_4$. The solution was maintained at 30 °C until **I-H$_4$** was almost completely cyclized (*ca.* 80%, see results) to **II-H$_2$**.

Other reagents (Merck, Aldrich or Sigma) were P.A. or spectroscopic grade and used as supplied. All aqueous solutions and buffers were prepared in freshly glass bi-distilled water. The buffers used were the sodium salts of borate (pH 9.0 to 10.0), phosphate (pH 6.4 to 8.0), acetate (pH 3.8 to 5.6), citrate (pH 2.2 to 6.0), 4-morpholineethanesulfonic acid, MES (pH 5.5 to 6.5), and [2-(hydroxymethyl) aminomethane], TRIS (pH 7.5 to 8.5). Buffer concentrations, shown in the figure legends, varied from 0.01 M to 0.05 M. HCl or $HClO_4$ were used for pHs lower than 2.0, and in the H_0 region.[18] $NaClO_4$ was obtained by neutralization of concentrated $HClO_4$ with sodium hydroxide.

2.2 Methods

UV-Vis absorption spectra and kinetic measurements were recorded using Hitachi U-2000, Cary 3E, Shimadzu UV-2401 PC or Beckman DU-7 spectrophotometers. Kinetic measurements were done at 30 °C ± 0.1. Fast reactions, above pH 7, were recorded in an Applied Photophysics Model SX-18 MV Stopped Flow system. Steady-state fluorescence spectra were recorded either in SPEX-1681 or Hitachi-F-2000 spectrofluorimeters. The excitation and emission slit widths were set to 1 mm, band-pass of 13 nm. Fluorescence emission spectra obtained with the SPEX fluorometer were corrected using the fabricant software. pHs were measured with a Beckman model Φ71 pH meter. **I** was titrated using a Radiometer PHM 82 Standard pH Meter equipped with a glass electrode calibrated with standard buffers at 30 °C.

Absorbance and fluorescence measurements. Absorption and fluorescence measurements were made using 3 mL quartz cuvettes with 10 mm optical path. Final concentrations of **III** or **I**, usually 1×10^{-5} M, were obtained by adding 1% (v/v) of the stock solution into the appropriate solvent or buffer. Stock solutions of **III** and **I** (1×10^{-3} M) were prepared in CH_3CN or DMSO and in aqueous NaOH respectively. The standard errors of the extinction coefficients were less than 5%.

Kinetic measurements. The kinetics of hydrolysis and cyclization were followed at the maximum absorbance wavelength as follows: 368 nm for **III** ($\varepsilon = 23\,737\ M^{-1}cm^{-1}$) and 308 nm for **I** ($\varepsilon = 10\,000\ M^{-1}cm^{-1}$). Reactions were initiated by adding 0.025 mL of stock solutions of the substrates to 2.5 mL of buffer giving a final concentration of 1.0×10^{-5} M. Rate constants were calculated from first-order kinetics with at least 4–5 half-lives in all cases and are the averages of at least three independent experiments differing by no more than 5%.

Fast kinetics. At each shot of the stopped flow system 0.1 mL of **III** stock solution in CH_3CN was mixed with 2.5 mL of buffer. Observed first-order rate constants, k_ψ, calculated by the SV18 MV program, are the mean values of at least 8 runs.

Potentiometric titrations. **I-Base** was titrated with 0.1148 M HCl, under N_2, using 50 mL of a 0.001 M solution of **I-Base** prepared in NaOH (pH 11.5). Titrant HCl was added to the solution with a Hamilton micro-syringe in volumes from 25 to 500 μL. All potentiometric titrations of **I-Base** were completed in *ca.* 15 min in order to minimize cyclization (see results). Data (pH *vs.* acid volume) were linearized with modified Gran functions to obtain pK_as values.[19]

Spectrophotometric titrations. The p$K_{II\text{-}1}$ and p$K_{II\text{-}2}$ of **II** were determined from the absorbance (365 nm) measured at several pHs, by adding 50 μL of 1×10^{-3} M solution of **II**, prepared at pH 1.0, to 2.0 mL of 0.05 M buffer at several pHs.

p$K_{I\text{-}H1}$ and p$K_{I\text{-}H2}$ of **I** were determined from measurement of the absorbance (at 250 nm), at several pHs, by adding 40 μL of 1×10^{-3} M of **I-Base**, prepared at pH 11.5, to 2.0 mL of 0.05 M buffer. The absorbances were measured within intervals of 30 s to minimize cyclization.

All kinetic reactions, titrations and equilibrium measurements were performed at 30 °C. **I** was also titrated by fluorescence (emission 454 nm, excitation 290 nm).

Structural calculations. Geometry optimization was performed by DFT level of theory using perturbed BP; DN** (Spartan v5).[20]

3 Results and discussion

3.1 Spectra

Typical UV-Vis absorption and fluorescence emission spectra of **III** are presented in Fig. 1. The UV maximum absorbance wavelengths, λ_{max}, and corresponding molar absorptivities, ε, of **III** in carbon tetrachloride and acetonitrile are collected in Table 1. The value of ε of **III** in CH_3CN (363.5 nm), is 30 618 M^{-1} cm^{-1}, a typical value of π, π* transitions, indicating a highly conjugated aromatic system. Spectral resolution of **III** and high ε values were similar to that observed for 1,4,5,8-naphthalene derivatives.[21]

Emission and excitation spectra of **III** in CH_3CN showed fine vibrational structure and were symmetric, demonstrating that the ground and excited states have the same geometry (Fig. 1A). Fluorescence quantum yields, Φ_f, and maximum emission wavelength, $\lambda^{em}{}_{max}$, of **III** in CH_3CN and CCl_4 are presented in Table 2. The low Φ_f value of **III** in CCl_4 can be attributed to a solvent quenching effect.[22]

The fluorescence spectra (emission and excitation) of **III** in a mixture of 50% CH_3CN–water changed with time (Fig. 1A). This effect is assigned to a hydrolysis reaction which leads to opening of the anhydride moiety and to a decrease in the aromatic conjugation

Table 1 Absorption maximum wavelengths (λ_{max}) and molar absorptivity coefficients (ε) of **III** in several solvents

Solvent	λ_1/nm	ε_1/$M^{-1}cm^{-1}$	λ_2/nm	ε_2/M^{-1} cm^{-1}	λ_3/nm	ε_3/$M^{-1}cm^{-1}$
CH_3CN	329	13 214	345.5	23 410	363.5	30 618
CCl_4	329	10 189	346	18 600	364	25 294
$HClO_4$ 0.1 M	332	11 708	348	19 699	368	23 737
$HClO_4$ 0.1 M + $NaClO_4$ 4 M	333	12 215	351	18 607	370	17 784
$HClO_4$ 12 M	336	11 700	354	20 751	375	25 552

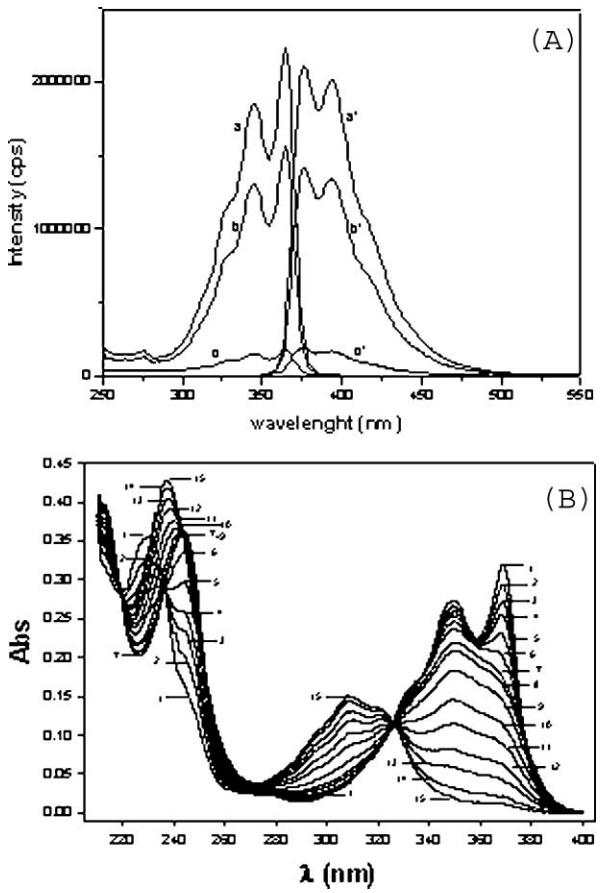

Fig. 1 (A) Fluorescence excitation (a, b, c) and emission (a′, b′, c′) spectra of **III**, 1×10^{-5} M, in acetonitrile–water (1:1 v/v) at different times, in minutes: zero (a, a′), 8 (b, b′) and 45 (c, c′). (**B**) UV-Vis spectra of **III**, 1×10^{-5} M, in phosphate buffer, 0.02 M, pH 7, as a function of time: (1) t = zero; (2) $t = 6$ s; (3) $t = 12$ s; (4) $t = 18$ s; (5) $t = 30$ s; (6) $t = 54$ s; (7) $t =$ 5 min; (8) $t = 9$ min (9) $t = 20$ min; (10) $t = 40$ min; (11) $t = 1$ h; (12) $t =$ 1.5 h; (13) $t = 2$ h; (14) $t = 3$ h; (15) $t = 4$ h.

Table 2 Fluorescence parameters for **III** in CH_3CN and CCl_4

Solvent	λ_1/nm[a]	λ_2/nm	λ_3/nm	Φ_f[b]
CH_3CN	372	390	414	0.130
CCl_4	369	389	415	0.015

[a] λ_1, λ_2, λ_3 are the emission maximum wavelengths (excitation wavelength λ was 330 nm). [b] Φ_f = Quantum yield.

extent and consequently in a decrease in Φ_f. Using methanol or ethanol as solvents, a time dependent shift was observed in **III** absorption λ_{max} from 368 nm to 346 nm, also indicative of solvolysis (not shown).

Like in other solvents (Table 1) compound **III**, as its diimide homologues,[21] showed a well-resolved UV-Vis absorbance spectrum in aqueous solution (phosphate buffer 0.02 M, pH 7.0) (Fig. 1B, line 1). The UV-Vis spectrum of **III** in water exhibits a λ_{max} at 368 nm and a second peak at 348 nm, similar to that obtained for films of **III**.[23] These features show that, as dianhydride or diimide, the chromophoric group remains relatively unsolvated.

Adding **III** to aqueous buffer (pH 7.0) resulted in a time-dependent spectral change (Fig. 1B). The absorbance at 368 nm (Fig. 1B) shows a rapid decrease, with half-life of *ca.* 24 s followed by a much slower process with a half-life of *ca.* 2 h which leads to further decrease in the absorbance at 368 nm and an increase in absorbance at 308 nm. The initial fast decrease in the absorbance at 368 nm is attributed to hydrolysis of **III** yielding **II** (Scheme 1). Compound **II** at pH 7 is almost completely dissociated (see below) and the fully dissociated ionic form of **II** will be referred as **II-Base**, (Scheme 1, and see below). Note that, in this initial reaction, an isosbestic point at 338 nm is evident (Fig. 1B). Above 260 nm the UV spectrum of **II-Base** shows a single λ_{max} at 348 nm (Fig. 1B, line 7). The slower process can be attributed to base catalyzed hydrolysis of **II-Base** yielding **I** (Fig. 1B, line 15), which at pH 7.0 is also fully dissociated, **I-Base**, see below (Scheme 1). The spectrum of **I-Base** exhibits a λ_{max} at 308 nm. In the alkaline hydrolysis of **II** → **I** an isosbestic point at 326 nm is clear.

In the following section a kinetic study of the reactions **III** → **II** and **II** ⇌ **I** in a wide range of acidities are presented.

3.2 Kinetics

The first order rate constant, k_ψ, for the reaction **III** → **II** was calculated from the absorbance change followed at 368 nm (where **III** absorbs) using only the fast change process. The variation of the observed rate constants, k_ψ, for the alkaline hydrolysis of **III** yielding **II-Base** with pH is shown in Fig. 2A. The solid line in Fig. 2A was obtained by fitting the data with eqn (1), where k_w is the first order rate constant for the water-catalyzed reaction and k_{OH} the second-order rate constant for hydroxide attack (**III** → **II-Base**, Scheme 1). The best-fit parameters were: $k_w^{III} = 0.005$ s^{-1} and $k_{OH}^{III} = 8.5 \times 10^4$ M^{-1}s^{-1}.

$$k_\psi = k_w + k_{OH}[OH] \quad (1)$$

The k_ψ for the water-catalyzed hydrolysis and hydroxide attack on **II-Base** yielding **I-Base**, were obtained starting the reaction by addition of **II-Base** to solutions of different pHs (insert, Fig. 2A). Using eqn (1) the best-fit parameters were $k_w^{II} = 2.0 \times 10^{-4}$ s^{-1} and $k_{OH}^{II} = 4.5 \times 10^2$ M^{-1} s^{-1}. The k_w^{III}/k_w^{II} and k_{OH}^{III}/k_{OH}^{II} ratios (25 and 190, respectively) show the difference in reactivity between the dianhydride and monoanhydride towards water and OH^-.

Addition of **III** to buffers of pHs between 1 and 6, also led to a time dependent changes in λ_{max} from 368 nm to 348 nm and a slower change from 348 to 308 nm (not shown). The fast process can be attributed to hydrolysis of **III** to **II** as analyzed above. The slower process, however, is more complex, since the UV spectra of the products correspond to **II** ⇌ **I** equilibrium mixture and the concentration of **I** at equilibrium was pH-dependent, decreasing with acidity (see below).

The time-dependent spectrum of a reaction mixture in 0.1 M $HClO_4$, with **III** as the initial reagent, is shown in Fig. 2B. Two consecutive isosbestic points can be differentiated: one at 341 nm during the fast first absorbance decrease and another at 320 nm in the slower phase. The existence of two consecutive isosbestic points lends credence to our assumption that the observed kinetics can be best explained by two consecutive reactions also at this pH, *i.e.* **III** → **II** and **II** ⇌ **I**. The peak at λ_{max} of **III** disappears after *ca.* 10 min (Fig. 2B) therefore, at equilibrium the spectrum corresponds to that of **II**, with a small contribution of **I**. It is also clear from the spectra that in the 1–6 pH range the final concentration of **III** is negligible.

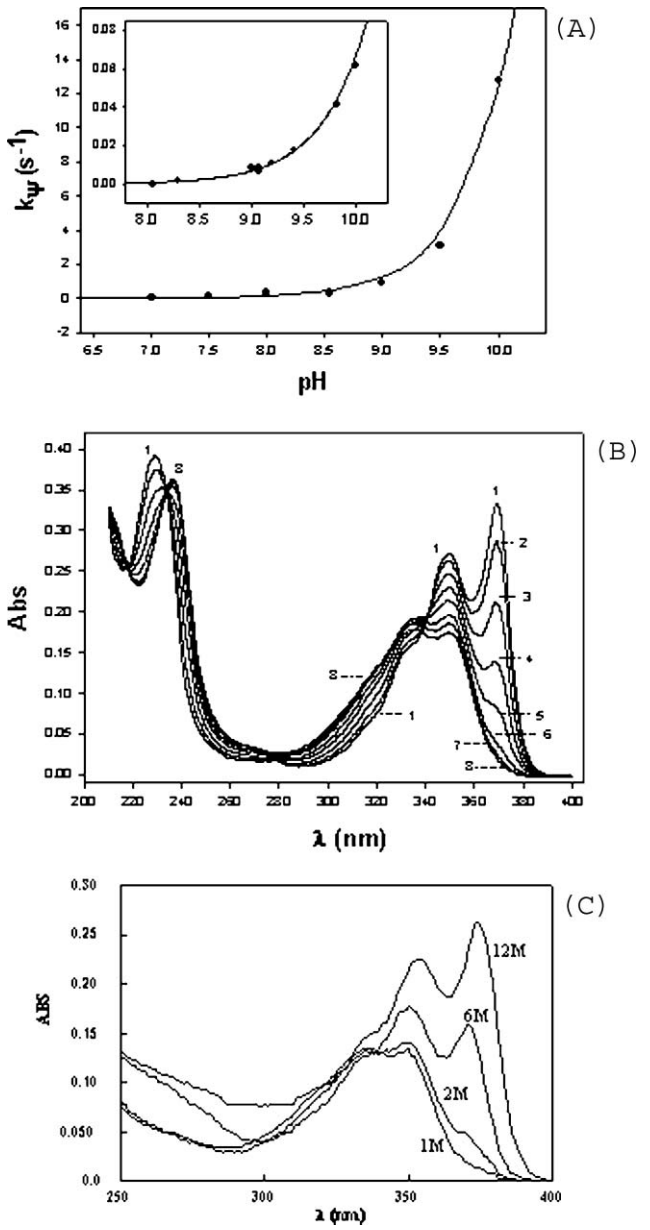

Fig. 2 (A) pH effect on k_ψ of hydrolysis of **III** to **II**. Inset: pH effect on k_ψ of hydrolysis of **II** to **I**. All buffers used were 0.02 M (see methods). The final concentrations of **II** and **III** were 1×10^{-5} M. Lines were calculated using eqn (1). (B) UV-Vis spectra of reaction mixtures of **III** in equilibrium with **II** as a function of time, in minutes, in 0.1 M $HClO_4$, pH = 1.0 at: (1) t = zero, (2) $t = 0.5$; (3) $t = 1.5$; (4) $t = 3$; (5) $t = 5$; (6) $t = 9$; (7) $t = 19$; (8) $t = 70$. The reaction was started with **I**. (C) Spectra at the end of reaction starting from **I-Base**, 1×10^{-5} M, in different [$HClO_4$].

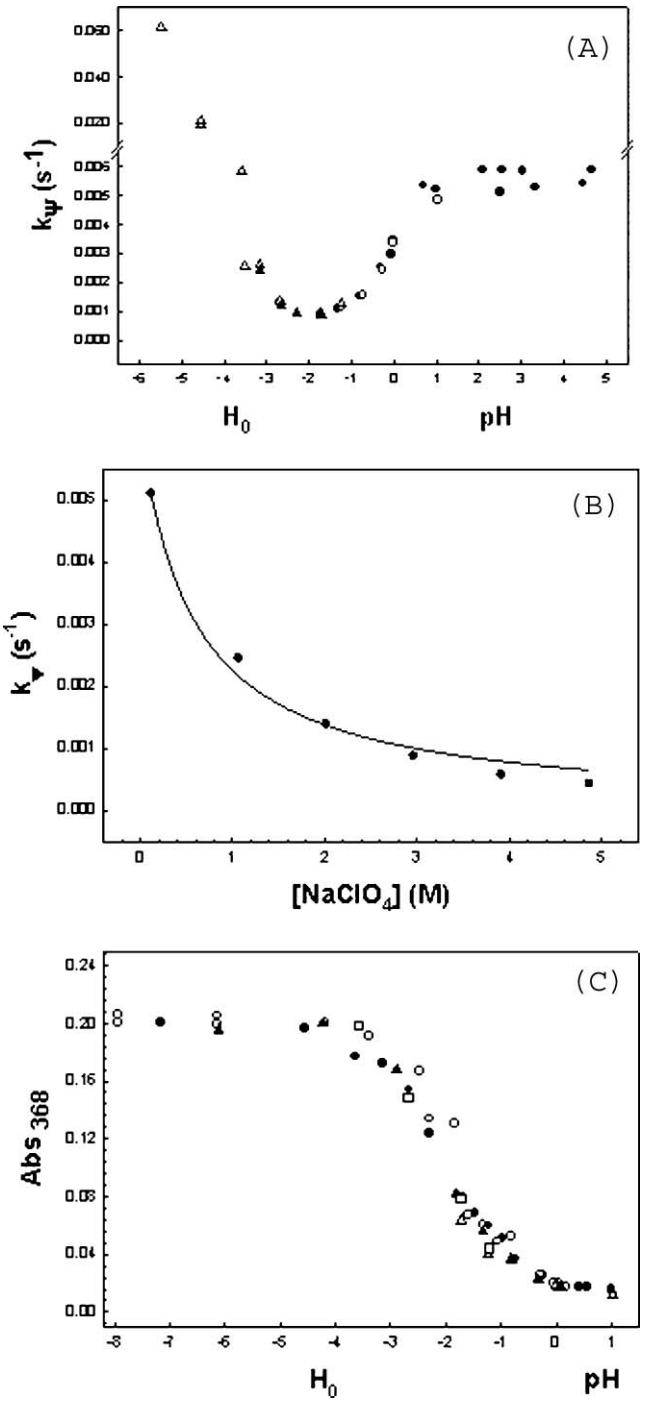

Fig. 3 (A) Effect of pH on k_ψ of reactions starting from **III** to **II** (○, ●, ▲) and starting from **II** to **III** (△). Different symbols correspond to different sets of experiments. Buffers used were 0.02 M. (B) Effect of [$NaClO_4$] on hydrolysis of **III** in $HClO_4$ 0.1 M. (C) Final absorbance, at 368 nm, after attainment of equilibrium, between **II** and **III** as a function of H_0, starting with [**II**] = 2.5×10^{-5} M. Different symbols correspond to independent sets of experiments (○, ●, ▲, △).

Above 1.0 M acid only the equilibrium between **III** and **II** was observed. The final spectrum of the reaction products, using either **III** or **II** or **I** as the initial reagent, shows a mixture of both compounds, with the **III**/**II** ratio increasing with [$HClO_4$] (Fig. 2C).

As described above, the rate constant, k_ψ, for hydrolysis of **III** yielding **II** can be obtained following the reaction at 368 nm. The variation of k_ψ with acidity was studied from pH 6 to $H_0 = -5$ and three different regions are evident (Fig. 3A). Between pH 6 to 0.5 k_ψ was constant, between pH 0.5 to $H_0 = -2$ k_ψ decreased with acidity to a minimum and below $H_0 = -2$, k_ψ increased with acidity.

Between pH 0.5 to 6, the reaction must be water catalyzed, since k_ψ did not vary with acidity and the value was identical to

that calculated for the water reaction with eqn (1) for the alkaline region (*i.e.*, $k_w^{III} = 0.005\ s^{-1}$) (Fig. 3A).

From pH 0.5 to $H_0 = -1.5$, k_ψ decreased with acidity and the product was also **II** (spectra, not shown). As described previously for the hydrolysis of anhydrides,[24] the decrease in k_ψ from pH 0.5 to −1.5 is due mainly to the increase in ionic strength. The effect of [$NaClO_4$] on the spectrum of **III** Table 1, and on k_ψ was determined in $HClO_4$ at several [$NaClO_4$]. As the concentration of acid increases there is a continuous shift in λ_{max} of **III** from 368 to 375 nm, due a combination of specific salt (*i.e.* ClO_4^-) effects, ionic strength and further protonation of **III** (Table 1). Addition of $NaClO_4$ (5.0 M) to a solution of **III** in 0.80 M $HClO_4$ red-shifted the λ_{max} from 368 to 372 nm (Table 1), indicating that part of the spectral changes observed in concentrated acid can be attributed to a medium polarity effect.

The value of k_ψ of the reaction (**III** → **II**) in 0.1 M $HClO_4$ decreased with [$NaClO_4$] from $5 \times 10^{-3}\ s^{-1}$ (no added salt) to $4.3 \times 10^{-4}\ s^{-1}$ (5.0 M $NaClO_4$) (Fig. 3B). This inhibitory salt effect, consistent with the decrease in observed in Fig. 3A in that acidity range, indicates that the minimum in the k_ψ *vs.* acidity plot results from ionic strength effect on the reaction.

Below H_0 −2 the hydrolysis of **III** is acid catalyzed, k_ψ increasing with H_0 (Fig. 3A). Further protonation of **III** and/or **II** can be proposed to rationalize these results. In order to ascertain that in the H_0 region **II** and **III** are in equilibrium we demonstrated that the value of the rate constants are identical upon starting the reaction with **II** or **III** (Fig. 3A).

The change in the spectra at the end of the reactions demonstrates the increase in **III**/**II** ratio with acidity (Fig. 2C). Upon increasing $HClO_4$, the spectrum approaches that of **III** and the absorbance at 368 nm, at the end of the reaction, A_∞, increases, indicating that **III** is the major equilibrium product (Fig. 3C). The equilibrium constant (**II** ⇌ **III**) was not calculated because the spectral changes reflect not only alteration in the **III**/**II** ratio but also the effects of ionic strength in the λ_{max} and ε of **III**. It is clear, however, that the equilibrium **II** ⇌ **III** is strongly displaced towards the dianhydride.

It has not escaped our attention that the use of the H_0 function is subject to debate.[25a] The H_A function may be more appropriate to describe the variation of both rate constant and absorbance with acid concentration in our system.[25b,c,d] The differences between using several functions to describe the effect of concentrated acid are evident,[25e] but no difference between H_A and H_0 is obtained, in our data, in the region where the minimum in the rate constant was obtained (Fig. 3A). We have thus used the H_0 function as a descriptive tool rather than as a method to rationalize mechanism or calculate values of equilibrium constants in concentrated acid.

The rate constants for reaching equilibrium in the **I** ⇌ **II** reaction and the final reaction spectra were determined between pHs 1 and 6. Both rate constants and final spectra were identical upon starting the reaction(s) with either reagent. When using **I** as a reagent we added an aliquot of **I-Base**, prepared by complete **III** hydrolysis at pH 10.2, to solutions of buffers at pHs < 6. A time-dependent change of spectra was obtained with λ_{max} changing from 308 nm to 348 nm, indicating formation of **II**. Final spectra of these reactions, at several pHs, are presented in Fig. 4A. The absence of a peak at 368 nm indicates no significant formation of **III** in this pH range. As the acidity increases, the **II**/**I** ratio increases, as evidenced by the increase in absorbance at 348 nm

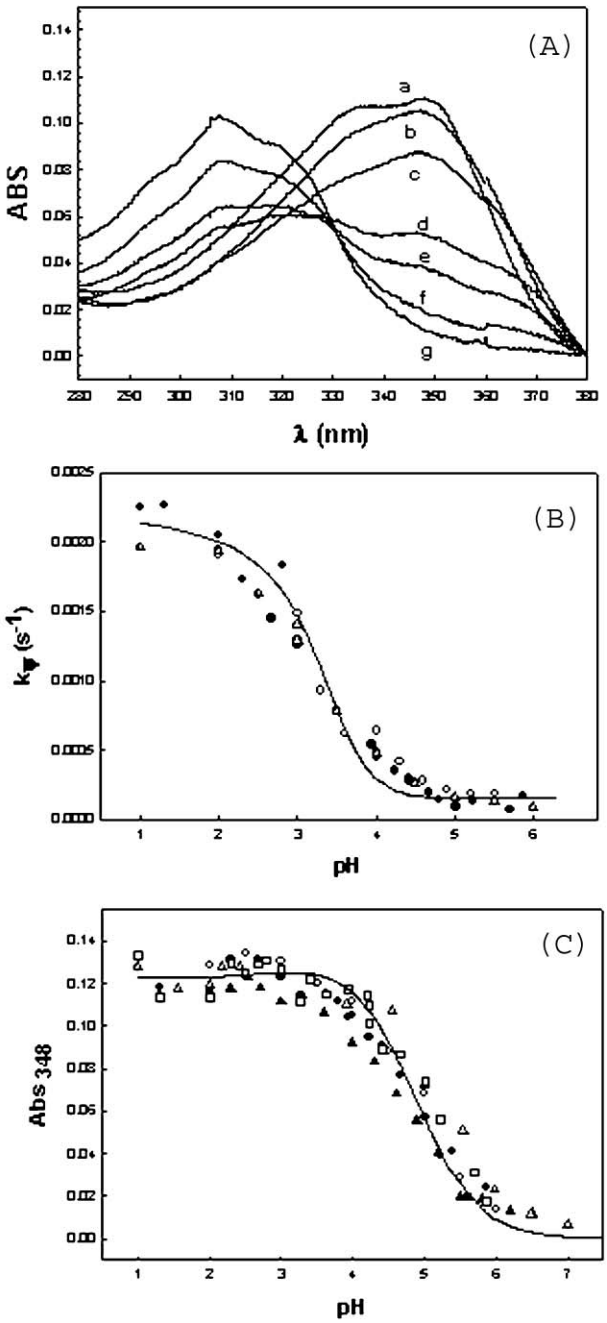

Fig. 4 (A) UV-Vis final spectra of cyclization of **I** to **II** at several pH's: (a) pH 2.3; (b) pH 3.0; (c) pH 4.0; (d) pH 4.9; (e) pH 5.2; (f) pH 5.5 and (g) pH 6.5. (B) pH effect on k_ψ of equilibrium reaction between **II** and **I**, starting from **I-Base**, followed at 348 nm and [**I-Base**] = 1.05×10^{-5} M. The solid line was obtained using eqn (14) and the different symbols correspond to independent sets of experiments. (C) pH effect on the absorbance at equilibrium between **II** and **I**, at 348 nm, starting the reaction from [**I-Base**] = 8.8×10^{-6} M. The different symbols correspond to independent sets of experiments. The solid line was obtained using eqn (10).

(Fig. 4A). The spectra of the final reaction mixture are complex because the carboxylic groups of **I** and **II** dissociate at this pH range (Scheme 1, see below) and the spectra, at each pH, reflects also the change in the concentration of ionic species of **II** and **I**.

The equilibrium constant for **II** ⇌ **I** reaction was measured at 348 nm. At this wavelength the ionic species of **II** have essentially the same absorption coefficient and absorption by **I** is insignificant (see below, Fig. 5B). Absorbance at the end of the reactions, A_∞, at this wavelength was used to calculate the equilibrium constant between (**II** ⇌ **I**) at several pHs (see below).

Below pH 6 the k_ψs for reaching equilibrium (**II** ⇌ **I**), followed at 348 nm, increased sigmoidally with pH, reaching a plateau at pH = 1 (Fig. 4B). The A_∞ of the reaction mixture plotted against pH increases with acidity to a plateau extending from pH 3 to pH 1 (Fig. 4C). The increase in k_ψ's and A_∞ with acidity led us to suggest that the protonated form of **I** is that involved in the cyclization to **II** and that formation of **II** is favored over **I** at low pH.

In order to determine the dissociation state of the species involved in the reactions of **I** and **II**, pK_as were determined.

3.3 pK_a Determination

The pK_as of **I** and **II** (Scheme 1) were determined by spectrophotometric and potentiometric methods. Protonation of **I-Base**, yields species **I-H**$_4$, **I-H**$_3$, **I-H**$_2$, **I-H** and **I-Base** and the corresponding pK_as are p$K_{\text{I-H4}}$, p$K_{\text{I-H3}}$, p$K_{\text{I-H2}}$, and p$K_{\text{I-H1}}$, respectively. It should be noted that the ionic species **I-H**$_2$ can correspond to different and indistinguishable isomers (**I-H**$_2$, **I-H**$_{2'}$) as shown in Scheme 1. The ionic forms of **II** are **II-H**$_2$, **II-H** and **II-Base** and the pK_as are p$K_{\text{II-H2}}$ and p$K_{\text{II-H1}}$, respectively.

Potentiometric titration allowed the determination of pK_as of **I** (see Methods). Titration data (pH *vs.* HCl volume) were treated by modified Gran functions (Fig. 5A).[19] The calculated pK_as of **I** were 3.24 ± 0.11, 5.13 ± 0.08 and 6.25 ± 0.05. Titration of a fully dissociated 1 mM solution of **I** with HCl (see Methods) needed 1.96 ± 0.36, 1.23 ± 0.09 and 1.16 ± 0.13 mM acid for full protonation at the above indicated pK_a regions. These data indicate a stoichiometry of 2 : 1 : 1, respectively (Table 3). The carboxylate dissociations around pH 3.2 can be attributed to those of the carboxylic groups at opposite sides of the naphthalene ring (p$K_{\text{I-H4}}$ and p$K_{\text{I-H3}}$, Scheme 1). The sensitivity of the titration method and the error in this pH region does not allow differentiation if those pK_as are identical or similar. Although **IH**$_4$ is neutral and **IH**$_3$ is negatively charged the pK_as can be similar. The dissociated carboxylate of **IH**$_3$ is at the opposite side of the naphthalene ring in relation to the carboxyl group that dissociates to yield **IH**$_2$.

IH$_3$ is highly conjugated and, furthermore, H bonding between the dissociated and protonated carboxylates of **IH**$_3$, at the same side of the ring, may decrease further the effect of the negative charge on the pK_a of **IH**$_3$ yielding **IH**$_2$. The pK_as 5.13 and 6.25 can be assigned to p$K_{\text{I-H2}}$ and p$K_{\text{I-H1}}$ (Scheme 1).

The different ionic species of **II** and **I** can also be differentiated spectrophotometrically, allowing faster pK_a determinations without significant cyclization.

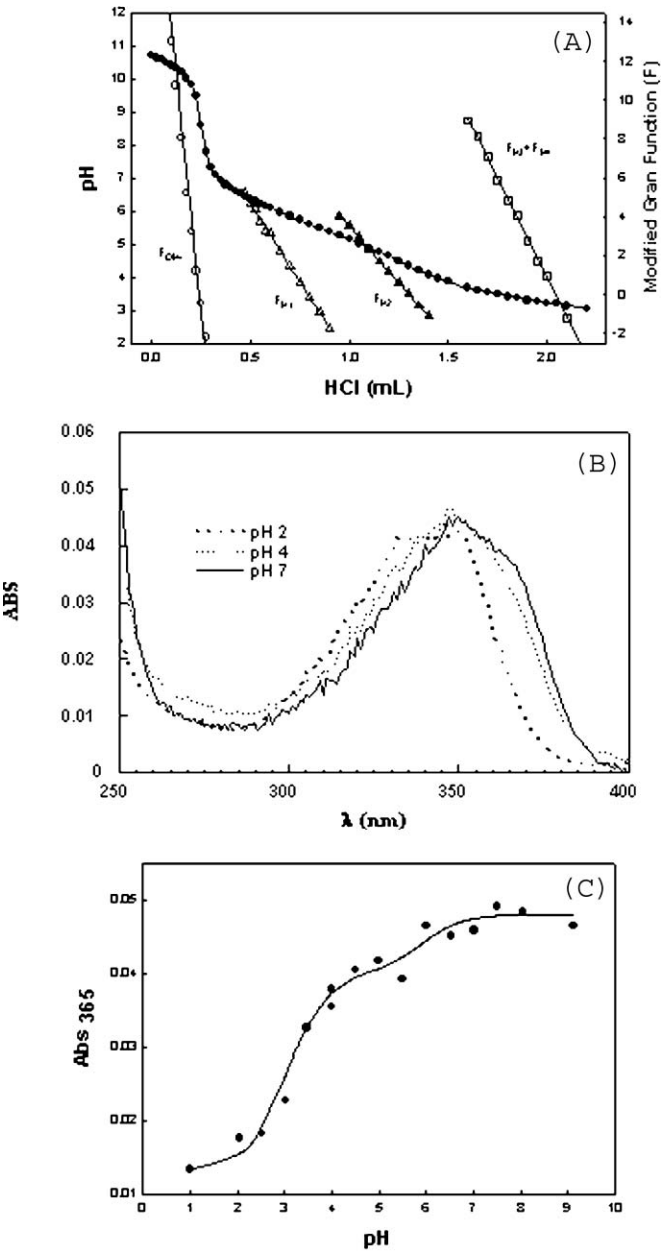

Fig. 5 (A) Experimental titration curve of **I** (●) linearized by the modified Gran functions (○) F_{OH^-} ($\times 10^3$), (△) F_{H1} ($\times 10^9$), (▲) F_{H2} ($\times 10^{10}$) and (□) $F_{H3} + F_{H4}$ ($\times 10^{12}$) with F_{OH^-}, F_{H1}, F_{H2} and $F_{H3} + F_{H4}$ corresponding to the titration of the excess of OH^- and ionizable groups with pK_as: 6.25 ± 0.05; 5.13 ± 0.08 and 3.24 ± 0.11, respectively. (B) pH effect on the absorbance spectra of **II**: (---) pH = 2; (• • •) pH = 4; (—) pH = 7. (C) pH effect on dissociation of **II**, 2.5×10^{-5} M, at 365 nm. Continuous line was generated using eqn (2). Buffer concentrations were 0.05 M.

Table 3 pK's of **I** and **II**

Method	p$K_{\text{II-H2}}$	p$K_{\text{II-H1}}$	p$K_{\text{I-H4}}$	p$K_{\text{I-H3}}$	p$K_{\text{I-H2}}$	p$K_{\text{I-H1}}$
Potentiometry			3.24 ± 0.11	3.24 ± 0.11	5.13 ± 0.08	6.25 ± 0.05
Fluorescence			3.65			
Equilibrium	3.40		3.70	3.70		
Kinetic	3.40		3.52	3.52		
UV Spectra	3.05	5.90				

The UV-Vis spectrum of **II** changes with pH upon deprotonation (Fig. 5B). The absorbance of **II** at 365 nm was recorded immediately after injecting an aliquot of **II** into buffered solutions in order to avoid ring opening. Absorbance *vs.* pH data are in Fig. 5C and the pK_as were calculated using the eqn (2):[10]

$$\text{Abs} = C_T \frac{\varepsilon_{\text{II-Base}} 10^{(\text{pH}-\text{p}K_{\text{II-H2}})} 10^{(\text{pH}-\text{p}K_{\text{II-H1}})} + \varepsilon_{\text{II-H}} 10^{(\text{pH}-\text{p}K_{\text{II-H1}})} + \varepsilon_{\text{II-H}_2}}{1 + 10^{(\text{pH}-\text{p}K_{\text{II-H1}})} + 10^{(\text{pH}-\text{p}K_{\text{II-H1}})} 10^{(\text{pH}-\text{p}K_{\text{II-H2}})}} \quad (2)$$

where Abs is the absorbance at 365 nm at each pH, C_T is the total concentration of **II**, $\varepsilon_{\text{II-Base}}$, $\varepsilon_{\text{II-H}}$ and $\varepsilon_{\text{II-H2}}$ are the molar extinction coefficient of the species (Scheme 1). The fit of eqn (2) to the experimental data in Fig. 5C yields a $\text{p}K_{\text{II-1}} = 3.05$ and $\text{p}K_{\text{II-2}} = 5.9$, Table 3, in good agreement with those obtained of 1,8-naphthalene diacid.[10]

The pH-dependent change of the maximum fluorescence wavelength of **I-Base** (data not shown) was attributed to changes in the protonation of the carboxylic groups. Only one pK_a could be determined by fluorescence, at 454 nm, with a value of 3.65 (Table 3).

Considering the differences in the methods used, the pK_as of **I** obtained by different methods agree very well (Table 3).

3.4 Quantitative analysis of equilibria

Since the absorptivity at 348 nm of **II-Base**, **II-H** and **II-H$_2$** are similar (Fig. 5B), this wavelength was used to measure the equilibrium constant between **II** and **I**, $K_{\text{Eq-II}}$. At 348 nm the absorption of **I** is less than 5% of that of compound **II** and can be neglected.

An initial estimation of $K_{\text{Eq-II}}$ between **I-H$_4$** and **II-H$_2$** was obtained from the following experiment: an aliquot of 0.05 mL of **III**, 1×10^{-3} M in DMSO, was added to 2.5 mL of a 0.02 M phosphate buffer, pH 7.1, and allowed to react for 3 min, yielding **II-Base** (the half life of this reaction is 24 s). At this time, 0.02 mL of 12 M $HClO_4$ were added to lower the pH to 1.3. At this pH **II** is in the fully protonated form, **II-H$_2$** (Table 3). The absorbance obtained after $HClO_4$ addition was used to calculate $\varepsilon_{\text{II-H2}}$ and the reaction was allowed to reach equilibrium, where a mixture of **II-H$_2$** and **I-H$_2$** was obtained. **I-H$_4$** does not absorb at this wavelength and, therefore, $K_{\text{Eq-II}}$ is given by:

$$K_{\text{Eq-II}} = \frac{\text{Abs}_f}{[\text{ABS}_i - \text{Abs}_f]} \quad (3)$$

where Abs_i is the initial absorbance of **II** at pH 1.3, Abs_f is the final absorbance of **II** at equilibrium and $(\text{Abs}_i - \text{Abs}_f)$ is equivalent to the concentration of **I**. The values of $\varepsilon_{\text{II-H2}}$ and $K_{\text{Eq-II}}$ were 16 715 M^{-1} cm^{-1} and 5.6 respectively.

The effect of pH on the [**II**]/[**I**] ratio was determined by measuring the A_∞ of the reaction as a function of pH. A_∞ was measured by adding **III** in DMSO to buffers with different pHs. **III** yields **II**, that subsequently equilibrates with **I**. The absorbance at equilibrium (**II** $\rightleftharpoons$ **I**) are in Fig. 4C. The decrease in pH led to the increase of A_∞, corresponding to an increase in the **II-H$_2$**/**I-H$_4$**ratio. The definitions of the dissociation equilibrium shown in Scheme 1 are in eqn (4)–(7).

$$K_{\text{Eq-II}} = \frac{k_1}{k_{-1}} = \frac{[\text{II-H}_2]}{[\text{I-H}_4]} \quad (4)$$

$$K_{\text{II-H2}} = \frac{[\text{II-H}][\text{H}^+]}{[\text{II-H}_2]} \quad (5)$$

$$K_{\text{I-H4}} = \frac{[\text{I-H}_3][\text{H}^+]}{[\text{I-H}_4]} \quad (6)$$

$$K_{\text{I-H3}} = \frac{[\text{I-H}_2][\text{H}^+]}{[\text{I-H}_3]} \quad (7)$$

Between pH 0 to 5, where the concentration of **III** at equilibrium is negligible, the total concentration of reagents, C_T is given by eqn (8):

$$C_T = [\text{I–H}_4] + [\text{I–H}_3] + [\text{I–H}_2] + [\text{II–H}_2] + [\text{II–H}] \quad (8)$$

As commented on above, the absorbance at equilibrium at 348 nm, Abs_∞, at each pH, is given by the sum of the absorbance due only to **II-H** and **II-H$_2$** because the ionic forms of **I** do not contribute to the absorbance at this wavelength:

$$\text{Abs}_\infty = \varepsilon_{\text{II-1}}[\text{II–H}] + \varepsilon_{\text{II-2}}[\text{II-H}_2] \quad (9)$$

where $\varepsilon_{\text{II-1}}$ and $\varepsilon_{\text{II-2}}$ are the absorption coefficients. $\varepsilon_{\text{II-1}}$ and $\varepsilon_{\text{II-2}}$ are essentially equal (Fig. 5B) and only one value for the coefficient was used here ($\varepsilon_{\text{II-1,2}}$).

$$\text{Abs}_\infty = \frac{C_T \varepsilon_{\text{II-1,2}} \left(1 + \frac{K_{\text{II-H2}}}{[\text{H}^+]}\right)}{1 + \frac{K_{\text{II-H2}}}{[\text{H}^+]} + \frac{1}{K_{\text{Eq-II}}} + \frac{K_{\text{I-H4}}}{[\text{H}^+]K_{\text{Eq-II}}} + \frac{K_{\text{I-H4}}K_{\text{I-H3}}}{[\text{H}^+]^2 K_{\text{Eq-II}}}} \quad (10)$$

The values of $\text{p}K_{\text{I-H4}}$, $\text{p}K_{\text{I-H3}}$, $\text{p}K_{\text{II-H2}}$ and $K_{\text{Eq-II}}$, were obtained by fitting the data in Fig. 4C using eqn (10). The solid line in Fig. 4C was obtained with the following values: $C_T = 8.8 \times 10^{-6}$ M, $\varepsilon_{\text{II-1,2}} =$ 16,715 M^{-1} cm^{-1}, $K_{\text{II-H2}} = 4 \times 10^{-4}$ ($\text{p}K_{\text{II-2}} = 3.4$), $K_{\text{I-H4}} = K_{\text{I-H3}} =$ 2.0×10^{-4}, ($\text{p}K_{\text{I-H4}} = \text{p}K_{\text{I-H3}} = 3.7$) (Table 3). The best fit value for $K_{\text{Eq-II}}$ was 5.0.

3.5 Quantitative analysis of kinetics

From the data presented above it can be concluded that the ionic species involved in the reaction **I** $\rightleftharpoons$ **II** are **I-H$_4$** and **II-H$_2$**. Between pH 1 and 3, the concentration of **II** at equilibrium is pH independent (Fig. 4C). Hence, it is reasonable to conclude that equilibrium is established between species **I-H$_4$** and **II-H$_2$**, *i.e.* between the fully protonated tetra-acid and the di-protonated mono-anhydride.

The **II**/**I** ratio at equilibrium is negligible above pH 5 (Fig. 4B), supporting the equilibrium data that also indicated that only **I-H$_4$** cyclizes. As only **I-H$_4$** cyclizes the system can be described as follows:

$$\frac{\text{d}[\text{II-H}_2]}{\text{d}t} = -\text{d}\frac{[\text{I-H}_4]}{\text{d}t} = k_1[\text{I-H}_4] - k_{-1}[\text{II-H}_2] \quad (11)$$

where k_1 and k_{-1} are the rate constants for formation and decomposition of **II-H$_2$** from **I-H$_4$** respectively, Scheme 1. The total concentration of **I**, $[\text{I}]_T$, and **II**, $[\text{II}]_T$, below pH 5, can be described by eqn (12) and (13).

$$[\text{I}]_T = [\text{I-H}_2] + [\text{I-H}_3] + [\text{I-H}_4] \quad (12)$$

$$[\text{II}]_T = [\text{II-H}_2] + [\text{II-H}] \quad (13)$$

The ionic forms **I-H**, **I-Base** and **II-Base**, and the respective dissociation constants, need not be considered, since their concentrations are negligible at pH < 5. Using eqn (4)–(7) and (11)–(13), the value of k_ψ is:

$$k_\psi = \frac{k_1[H^+]^2}{\left([H^+]^2 + K_{I\text{-}H4}[H^+] + K_{I\text{-}H4}K_{I\text{-}H3}\right)} + \frac{k_{-1}[H^+]}{([H^+] + K_{II\text{-}H2})} \quad (14)$$

The fit of eqn (14) to the kinetic data in Fig. 4B was obtained using $k_{-1} = 0.000275$, $k_1 = 0.00165$ and $K_{II\text{-}2} = 4 \times 10^{-4}$ ($pK_{II\text{-}2} = 3.4$), $K_{I\text{-}H4} = K_{I\text{-}H2} = 3 \times 10^{-4}$ ($pK_{I\text{-}H4} = pK_{I\text{-}H3} = 3.52$). The ratio between k_1 and k_{-1} yields the equilibrium constant, $K_{Eq\text{-}II}$, eqn (3). The best-fit value of the kinetic data was obtained with $K_{Eq\text{-}II} = k_1/k_{-1} = 6$, in good agreement with that obtained from the equilibrium data, *i.e.*, $K_{Eq\text{-}II} = 5$.

These results led us to conclude that protonation of the four carboxylic acids of **I** is necessary for, at least, one ring cyclization leading to **II-H$_2$**. The value of $K_{Eq\text{-}II}$ indicates that **II** is favored over **I** at low pH, in agreement with the previous data for cyclization of 1,8-naphthalic dicarboxylic acid to the anhydride ($K_{Eq} = 3$ at 30 °C).[10]

3.6 Structural calculations

Our kinetic and equilibrium data showed unequivocally a major decrease in reactivity upon opening of the first anhydride (*i.e.*, compare the rates of reaction of **III** to **II** with those from **II** to **I**) from pH 2 to pH 7, *i.e.* water reaction, and in alkali. Furthermore, it was evident that the monoanhydride **II** was reversibly transformed into dianhydride **III** only at high [H$^+$]. It was of interest to obtain independent structural data supporting these experimental observations. For this purpose we calculated the electronic density maps of geometry optimized structures (see Methods) in the gas phase. Calculations, performed exclusively for the first ring opening, were done separately for the acid, water and base-catalyzed reaction manifolds (Schemes 2–4).

Schemes 2–4 show some model structures possibly involved in the acid, base and water catalysis of hydrolysis of **III**. The color intensities depict electronic isosurfaces referring to each structure. Relative color intensities, from one structure to another, cannot be compared. Selected values of electrostatic potential at the same of the atoms in the structures shown in Schemes 2–4 are presented in Table 4 for clarity.

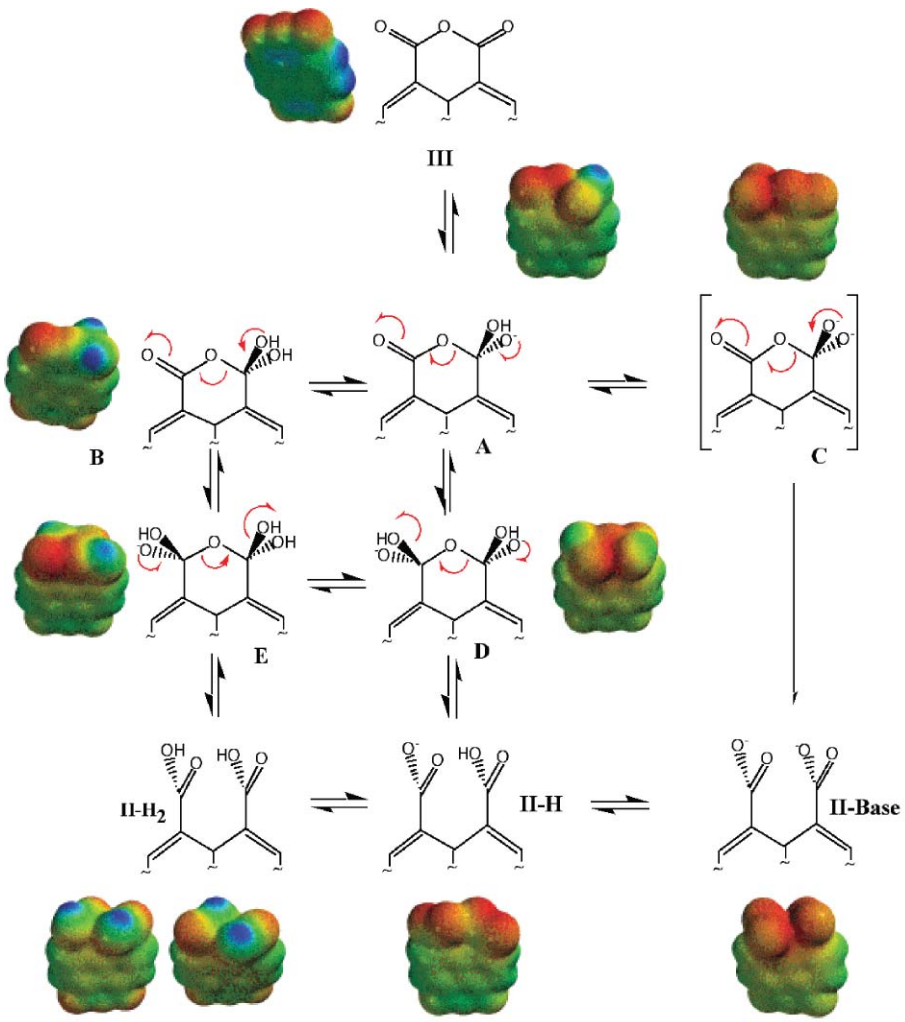

Scheme 2 Mechanism of alkaline hydrolysis of **III**.

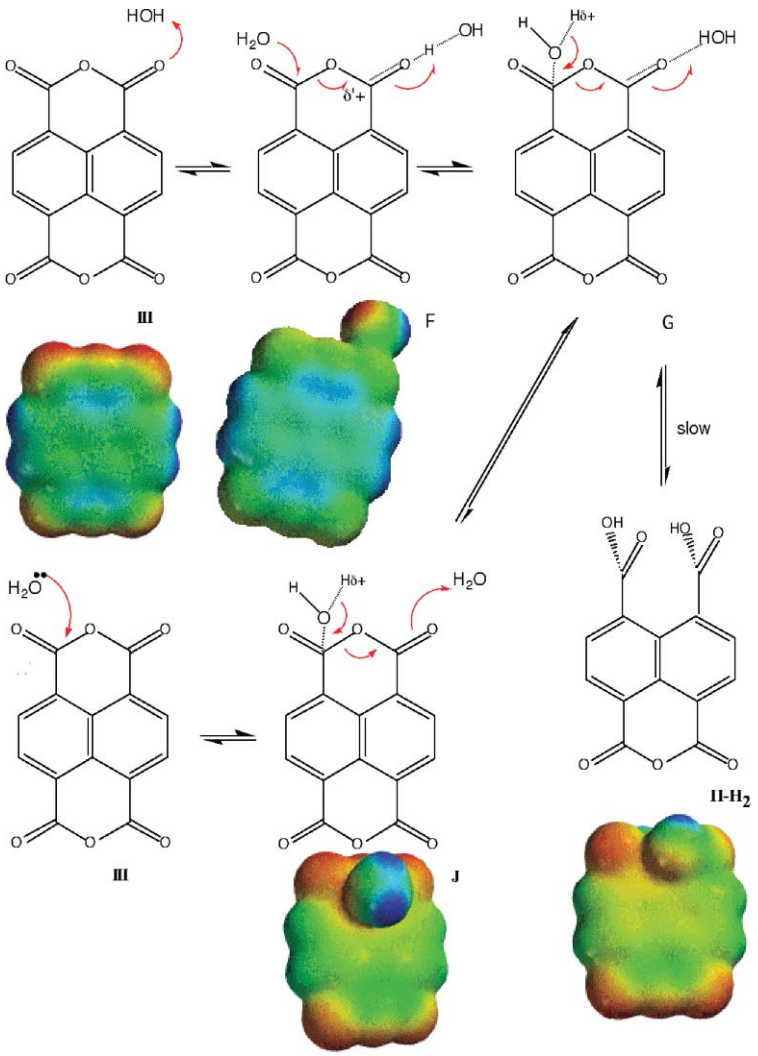

Scheme 3 Mechanism of water hydrolysis of **III**.

Table 4 Electrostatic potential at some regions of molecular structures defined in Schemes 2–4

Structures	V^+ (kcal mol^{-1})[a]	V^- (kcal mol^{-1})[b]	V$^+$ (kcal mol^{-1})[c]
A	−59		
B	9		
C	−126		
D	−135		
E	−62		
II-H$_2$	8 (*trans*); 8 (*cis*)	−41 (*trans*); −41 (*cis*)	
II-H	−56		
II-Base	−131		
F	19		18
J	14	−36	
K		15	98
L		12	
III	17	−33	

[a] Potential at carbonyl carbon in the opposite side of reaction center. [b] Potential at carbonyl oxygen in the opposite side of reaction center. [c] Potential at carbonyl carbon in the same side of reaction center.

Scheme 2 shows the geometry optimization calculations for the presumed intermediates formed upon OH^- attack on **III**. Although the calculated structures in base were not detected here by UV absorption in water, structure **B** in aprotic DMSO had been observed by IR and ^{1}H NMR spectroscopy.[26] In a highly conjugated molecule such as **III**, hydroxide addition to one of the carbonyl carbons increases the electronic density along the whole structure. This is demonstrated both by the density potential plots in Scheme 2 (compare **III** with intermediates and products) as well as the values of electrostatic potential (V^+) at the carbonyl carbon centered at the opposite side of the reaction (Table 4). Hence we chose to calculate simple model structures, starting material and those most likely to be formed along the reaction pathways, excluding more complex, water bridged models. It should be noted that **III**, although containing six oxygen atoms and four carbonyls, is poorly water soluble and that the calculated electrostatic potential at the carbonyl carbon of **III** does not vary significantly after inclusion of a hydrogen bonded water molecule (See Table 4). Our calculations do not allow decisions of preferred pathways but the methodological choice permitted estimation

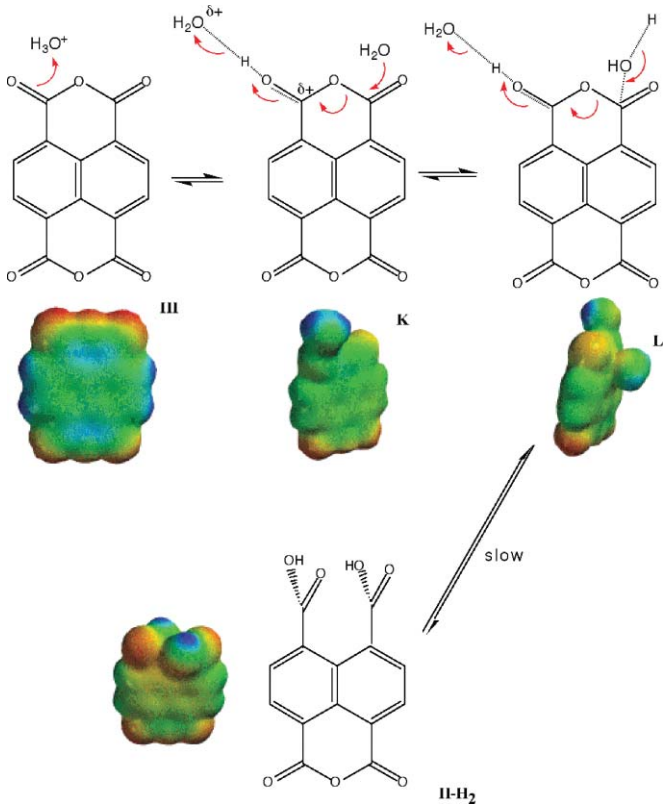

Scheme 4 Mechanism of acid hydrolysis of **III**.

of electronic correlation dependent properties. The calculations, as will be discussed below, were sufficiently accurate to permit better molecular level understanding of part of the experimental findings. Structures shown in Scheme 2, with the exception of **C** were stationary states, suggesting that a proton loss from **A** may lead to **II-Base** with no intervening intermediate. The electronic isosurface shown above **C** corresponds to that of **II-Base**. In the first proposed structure formed after OH^- attack to one of the carbonyl carbons, (**A**), we calculated extensive electronic availability along the molecular structure (Scheme 2, Table 4). The redistribution of charge in the molecule is maintained in the final product and while the value of the electrostatic potential at the carbonyl carbon of **III** was 17 kcal mol^{-1} that of **II-Base** was −131 kcal mol^{-1} (Table 4).

Although our calculations in the gas phase allow for the existence of **II-H$_2$**, **II-H** and **II-Base**, only **II-Base** is significant in alkali (see above). The increase in negative charge density at the carbonyl carbon of the remaining anhydride is in qualitative agreement with the 200 fold decrease in reactivity observed experimentally when reactions **III** to **II** and **II** to **I** in alkali are compared (see text).

From pH 2 to 7 the rate of anhydride hydrolysis remains unchanged, suggesting a water-catalyzed hydrolysis (see above). Water attack to the carbonyl carbon can be calculated from a solvated **III** (**F** in Scheme 3), similar to a protonated species in acid (**K** in Scheme 4). A H_2O–**III** complex, hydrogen bonded to a carbonyl oxygen, and a nucleophilic attack by water oxygen to carbonyl carbon, produces structures **F** and **G** (Scheme 3). The attempts to calculate structure **G** (Scheme 3) by correlated DFT level of theory failed, probably due to very weak interactions. A HF/6-31G* calculation did not result in reasonable distances for any significant interactions. Structure **F** (Scheme 3) presents a weak hydrogen bond with a water molecule, in agreement with the low water solubility of **III** in that pH range. In fact the small differences observed in the values of the electrostatic potential at the carbonyl carbon in the same side of reaction center of species **III** (17 kcal mol^{-1}) and **J** (18 kcal mol^{-1}) (Table 4) also indicate very small water–reagent interaction. In the assumed structure **J** (Scheme 3) the water O carbonyl C distance is large, and the contribution of this species can be neglected. The calculations shown in Scheme 3 suggest that the preferred pathway for water-catalyzed hydrolysis follows the pathway **III** ⇌ **F** ⇌ **II-H$_2$**. The rate difference between the **III** to **II** and **II** to **I** water-catalyzed reactions was 20 fold, an order of magnitude lower than that for the corresponding OH^- reactions of the same species. The calculated differences in electrostatic potentials also were correspondingly lower (Table 4).

The limited number of structures considered in acid suggests a straightforward protonation followed by water attack (Scheme 4).

4 Conclusions

Product composition and rates for the hydrolysis of **III** in aqueous solution varied significantly with acidity. In base **III** hydrolyzed to yield **II** and **I** and, at infinite time, the only significant product was **I**. In moderate acidic solutions the hydrolysis of **III** gave an **I** ⇌ **II** equilibrium mixture. **III** only equilibrates with **II** in concentrated acid. pK_a determinations using different methods and quantitative analysis of equilibrium and kinetic data permitted the full description of the hydrolysis of **III** from alkaline solutions to concentrated acid. Carboxylic acid protonation at the same side of the ring was demonstrated to be necessary for anhydride formation. The rates of water or hydroxide attack on the dianhydride **III** were significantly higher when compared to the monoanhydride **II**. Geometry optimization calculations clearly indicated that addition of a nucleophile to the dianhydride resulted in a redistribution of the electronic density over the whole molecule and were qualitatively consistent with the observed reactivity differences between **III** and **II**. These results represent the first mechanistic description of the hydrolysis of **III** in aqueous solution over a wide range of conditions and contribute to the understanding of anhydride reactivity in highly conjugated systems.

Acknowledgements

Financial support for this work was received from CNPq, FAPESP, Pró-Reitoria de Pesquisa da USP and UNIP.

References and notes

1 T. C. Bruice and F. C. Lightstone, *Acc. Chem. Res.*, 1999, **32**, 127–136.
2 A. J. Kirby, *Adv. Phys. Org. Chem.*, 1980, **17**, 183–278.
3 W. P. Jencks, *Catalysis in Chemistry and Enzymology*, Dover, New York, 1987.
4 S. Y. Yunes, J. C. Gesser, H. Chaimovich and F. Nome, *J. Phys. Org. Chem.*, 1997, **10**, 461–465.
5 T. C. Barros, *Formação e Decomposição de Naftalimidas em Solução Aquosa: Dependência Estrutural e Efeito de Micelas*, Master Thesis, Chemistry Institute, Biochemical Department, University of São Paulo, USP, São Paulo, Brazil, 1991.
6 M. Bender, *Chem. Rev.*, 1960, **60**, 53–113.

7 J. A. Knopp, W. S. Linnell and W. C. Child, Jr., *J. Phys. Chem.*, 1962, **66**, 1513–1516.
8 W. P. Jencks, F. Barley, R. Barnett and M. Gilchrist, *J. Am. Chem. Soc.*, 1966, **88**, 4464–4467.
9 (*a*) L. Eberson, *Acta Chem. Scand.*, 1964, **18**, 1276–1282; (*b*) L. Eberson and H. Welinder, *J. Am. Chem. Soc.*, 1972, **93**, 5821–5826; (*c*) L. Higuchi, L. Eberson and J. D. McRae, *J. Am. Chem. Soc.*, 1967, **89**, 3001; (*d*) M. D. Hawkins, *J. Chem. Soc., Perkin Trans. 2*, 1975, 282.
10 T. C. Barros, S. Yunes, G. Menegon, F. Nome, H. Chaimovich, M. J. Politi, L. G. Dias and I. M. Cuccovia, *J. Chem. Soc., Perkin Trans. 2*, 2001, 2342–2350.
11 A. G. Kofman, G. V. Chernysh, V. A. Shingalevskii and G. N. Vorozhtsov, *Zh. Org. Khim.*, 1988, **24**, 1973–1978; A. G. Kofman, G. V. Chernysh, V. A. Shingalevskii and G. N. Vorozhtsov, *Zh. Org. Khim. (Engl. Transl.)*, 1989, 1778–1783.
12 L. Born and G. Heywang, *Z. Kristallogr.*, 1990, **190**, 147–152.
13 L. J. Fitzgerald, J. Gallucci and R. E. Gerkin, *Acta Crystallogr., Sect. C*, 1991, **47**, 2315–2319.
14 L. J. Fitzgerald, J. Gallucci and R. E. Gerkin, *Acta Crystallogr., Sect. C*, 1992, **48**, 460–465.
15 L. J. Fitzgerald, J. Gallucci and R. E. Gerkin, *Acta Crystallogr., Sect. C*, 1992, **48**, 1430–1434.
16 A. C. Blackburn, L. J. Fitzgerald and R. E. Gerkin, *Acta Crystallogr., Sect. C*, 1997, **53**, 1991–1995.
17 The commercial 1,4,5,8-naphthalene tetracarboxylic acid, **I**, (Aldrich) was not employed here because its absorption spectra in CH_3CN corresponds to the 1,4,5,8-naphthalene diacid monoanhydride, **II**, maximum at 348 nm and not to **I**, maximum at 308 nm.
18 R. H. Boyd, in *Solute Solvent Interactions*, ed. J. F. Coetzee and C. D. Ritchie, 1969.
19 J. C. Masini, *Talanta*, 1994, **41**, 1383–1389.
20 *Spartan Version 5.0*, Wave Function, Inc., 18401 Von Karman Avenue, Suite 370, Irvine, CA 92612 USA.
21 T. C. Barros, S. Brochsztain, V. G. Toscano, P. Berci Filho and M. J. Politi, *J. Photochem. Photobiol., A*, 1997, **111**, 97–104.
22 A. Gilbert, and J. Baggott, *Essentials of Molecular Photochemistry*, CRC Press, London, 1991.
23 A. Jayaraman, M. L. Kaplan and P. H. Schimidt, *J. Phys. Chem.*, 1985, **82**, 1682–1687.
24 C. A. Bunton, N. A. Fuller, S. G. Perry and I. H. Pitman, *J. Chem. Soc.*, 1962, 4478–4485.
25 (*a*) R. A. Cox and K. Yates, *Can. J. Chem.*, 1983, **61**, 2225–2243; (*b*) K. Yates and J. B. Stevens, *Can. J. Chem.*, 1964, **42**, 1957–1970; (*c*) R. A. Cox, C. R. Smith and K. Yates, *Can. J. Chem.*, 1979, **57**, 2952–2959; (*d*) R. A. Cox and K. Yates, *Can. J. Chem.*, 1979, **57**, 2944–2951; (*e*) K. Yates, H. Wai, G. Welch and R. A. McClelland, *J. Am. Chem. Soc.*, 1973, **95**, 418–426.
26 I. D. Rae, *Aust. J. Chem.*, 1972, **25**, 679–681.

